Short communication

Mg partitioning between solid and liquid iron under the Earth's core conditions

Yunguo Li*, Lidunka Vočadlo, Dario Alfè, John Brodholt

Department of Earth Sciences, UCL, Gower Street, London WC1E 6BT, UK

A B S T R A C T

Recent studies show the Earth's core may contain more magnesium (Mg) than previously thought, with perhaps up to 6 wt% in the early core and ~1 wt% still existing now. The Mg partitioning between liquid and solid iron (Fe) under the relevant conditions is needed, therefore, in order to establish whether the presence of magnesium will have an effect on core properties, particularly those of the inner core. Using the techniques of *ab initio* molecular dynamics (AIMD) and thermodynamic integration, we have calculated the chemical potential and partition coefficient of Mg between solid and liquid Fe at 360 GPa and 6500 K. We find Mg partitioning slightly favours liquid Fe but still allows a significant amount of Mg into the solid, which will likely make a small but important contribution to the light-element effects on core properties.

1. Introduction

The density of the Earth's core from seismic observations is about 10% lower than that of an iron-nickel (Fe-Ni) alloy at the relevant conditions (Poirier, 1994). Light elements are, therefore, expected in the core to account for the density deficit. However, despite many studies there is still no consensus as to which light element(s) are incorporated into either the inner or outer core (Alfè et al., 2000a; Badro et al., 2015; Li et al., 2016; Litasov and Shatskiy, 2016).

The crucial constraints are the core density and sound velocities. Any candidate light-element iron alloy must be able to match the inner-core and outer-core densities and sound velocities, consistent with equilibrium partitioning between (solid) inner and (liquid) outer core. The partition coefficients of light-element candidates are, therefore, essential for understanding the core. Previous work shows that silicon (Si) and sulphur (S) partition almost equally between the solid and liquid Fe under core conditions (Alfè et al., 2000a), while oxygen almost completely partitions into the liquid outer core (Alfè et al., 2000b, 2002b). While these are very likely candidates for the light elements in the core, no composition has yet been found in the Fe-Ni-Si-S-O system which simultaneously matches the inner-core and outer-core densities and sound velocities (Litasov and Shatskiy, 2016; Martorell et al., 2016).

Lithophile magnesium (Mg) is not usually considered as a main light-element candidate (Poirier, 1994) mainly because Mg and Fe are almost immiscible under ambient conditions (McDonough and Sun, 1995). Furthermore, it has recently been proposed that if there were

any Mg in the outer core in the early stages of the earth's evolution, most of it will have precipitated out of the core into the mantle in the form of Mg-bearing minerals during the differentiation process, thereby driving outer-core convection and providing a mechanism for magnetic field generation (O'Rourke and Stevenson, 2016).

However, there is now evidence that shows that substantial amounts of Mg may be dissolved into Fe at high temperatures and high pressures; indeed, at high temperatures, the entropic effects become sufficiently large that the solubility of Mg in Fe increases almost exponentially with increasing temperature (O'Rourke and Stevenson, 2016; Takafuji et al., 2005; Wahl and Militzer, 2015). Experiments have shown that 0.8 mol.% Mg was detected in quenched liquid iron in equilibrium with $(Mg,Fe)SiO_3$ perovskite at 95 GPa and 3050 K (Takafuji et al., 2005), while first-principles calculations have shown that the saturation limit of MgO in Fe increases from 0.1 mol.% at 3000 K to 1 mol.% at 4200 K and 50 GPa (Wahl and Militzer, 2015). Furthermore, a combined experimental and theoretical study has shown that the solubility of Mg in liquid Fe increases dramatically with increasing pressure, with the liquid Fe-Mg alloy containing more than 10 mol.% dissolved Mg at 126(3) GPa and 3650(250) K (Dubrovinskaia et al., 2005).

Recently, Badro et al. (2016) presented a core formation model based on experimental data which shows that there could have been as much as 6 wt% MgO dissolved in the liquid core at the core-mantle boundary in the early stages of core formation, but that this will have reduced significantly to ~1.1 wt% in the present day. While such a small amount of Mg is not likely to affect significantly outer-core

---

properties (where the light element component is ~10 wt%), such an amount could be important if Mg partitioned strongly into the inner-core, where the total light element contribution is significantly lower (only 3–4 wt%). There is good reason, therefore, to revisit the possibility of the presence of Mg in the core and address the potential visible effects on inner-core properties which could be expected, even from such small concentrations. This is the first time that the partitioning of Mg between the inner and outer core has been determined.

The amount of Mg in the inner core depends critically on the partitioning of Mg between solid and liquid Fe. In this paper, therefore, we have calculated the chemical potential of Mg in solid and liquid iron under core conditions using a combination of *ab initio* molecular dynamics (AIMD) and thermodynamic integration. From the chemical potentials, we obtained the partition coefficients. We find that Mg slightly favours the liquid, but also partitions significantly into the solid and therefore is likely to make an important contribution to the light element effects on inner core properties.

2. Methods

The methods used here for magnesium partitioning follow that detailed in the previous work of Alfè et al. (2002a) on the partitioning of sulphur, silicon and oxygen between solid and liquid iron at inner core conditions.

The chemical potential of the solute X in solvent A in the low-concentration limit can be written as

$$\mu_X(p,T,C_X) = k_B T \ln C_X + \overline{\mu}_X(p,T,C_X) \tag{1}$$

where $\overline{\mu}_X(p,T,C_X)$ is dependent on the molar fraction of solute (C_X) due to the interactions between solute atoms. A linear function can be assumed to take account of this interaction using $\overline{\mu}_X(p,T,C_X) = \mu_X^{\dagger} + \lambda_X(p,T)C_X$.

The ratio of the molar fraction C_X^s and C_X^l in solid and liquid is therefore determined by

$$C_X^s/C_X^l = \exp[(\mu_X^l - \mu_X^s)/k_B T_m] \tag{2}$$

The chemical potential of a solute is the change in Gibbs free energy when adding one solute atom to the system at constant pressure and temperature. In practical *ab initio* calculations, we chose to convert solvent into solute, so we obtain the difference between the solute and solvent chemical potentials $\mu_{XA} = \mu_X - \mu_A$ (then μ_X can be obtained by calculating the Gibbs free energy of pure solvent μ_A), which is equal to the change of Helmholtz free energy (F) of the system when we work at constant volume rather than at constant pressure

$$\mu_{XA} = F(N_A - 1, N_X + 1) - F(N_A, N_X)$$
$$= k_B T \ln(C_X) + 3k_B T C_X + 3k_B T \ln\left(\frac{\Lambda_X}{\Lambda_A}\right) + m(\overline{v}, T, C_X) \tag{3}$$

where $F(N_A, N_X)$ is the Helmholtz free energy of the system with N_A solvent atoms and N_X solute atoms, $F(N_A - 1, N_X + 1)$ is for the system with one less solvent atom and one more solute atom. Λ_X and Λ_A (calculated by $\Lambda_A = h/(2\pi M_A k_B T)^{1/2}$) are the thermal wavelengths of X and A, respectively, and $m(\overline{v}, T, C_X)$ can be calculated by the thermodynamic integration technique

$$m(\overline{v}, T, C_X) = \int_0^1 d\lambda \, <U_1 - U_0>_\lambda \tag{4}$$

with the potential functions $U_1(\mathbf{R}) = U(N_A - 1, N_X + 1; \mathbf{R})$ and $U_0(\mathbf{R}) = U(N_A, N_X; \mathbf{R})$.

As the thermodynamic integration is performed at constant volume, a correction to the constant pressure free energy can be made by

$$(\partial m(p,T,C_X)/\partial C_X)_P = (\partial m(\overline{v},T,C_X)/\partial C_X)_V - nB_T(v_X - v_A)^2 \tag{5}$$

where B_T is the bulk modulus, $n = \frac{N}{V}$ is the overall atomic number density, and v_X and v_A are the partial atomic volumes of solute and solvent, respectively. The partial atomic volume can be taken as the

change in volume of the whole system when one atom of X or Fe is added at constant P and T.

Another correction to the partition coefficient due to the deviation of melting temperature from that of pure solvent can be made by

$$C_X^s/C_X^l = \exp[(\mu_X^l - \mu_X^s)/k_B T_m]/\exp[(\mu_A^{0s} - \mu_A^{0l})/k_B T_m] \tag{6}$$

where μ_A^{0s} and μ_A^{0l} are the Gibbs free energies of pure solvent in solid and liquid forms at temperature T_m.

As for the previous calculations on Si, S, and O (Alfè et al., 2002a), we performed AIMD calculations on a supercell of 64 atoms to calculate the free energy change $m(\overline{v},T,C_X)$ and hence μ_{XA} in liquid Fe. The calculations were performed at ~360 GPa (corresponding to a volume/atom $V/N = 7.0$ Å³/atom) and 6500 K. For the solid, calculations were also performed at ~360 GPa (corresponding to a volume/atom $V/N = 6.9$ Å³/atom) and 6500 K. It is generally accepted that Fe takes the hexagonal-close-packed (*hcp*) structure under inner-core conditions, so a hexagonal supercell of 64 atoms was used. Thermodynamic integration was used to calculate $m(\overline{v},T,C_X)$ with $C_X = 0.015625$ for the solid and $C_X = 0.015625$ and 0.03125 for the liquid. We used five equally spaced λ (0.0, 0.25, 0.5, 0.75, and 1.0); five values of λ have previously been shown to be sufficient to converge the integration within the statistical error for similar calculations on Si, S and O (Alfè et al., 2002a). Indeed, in our present work, five values of λ proved to be more than enough, since the integrand $\langle U_1 - U_0 \rangle_\lambda$ in Eq. (4) used to calculate the free energy change $m(\overline{v},T,C_X)$ shows an almost linear dependence with λ (Fig. 1).

We ran finite temperature Born–Oppenheimer AIMD in the canonical ensemble. The Verlet algorithm was used (with a time step of 1.0 fs) to integrate the classical Newton's equations of motion. The temperature was controlled by a Nosé thermostat (Di Tolla and Ronchetti, 1993; Nosé, 1984). We used VASP code (Blöchl, 1994; Kresse and Joubert, 1999), PAW potentials (Kresse and Hafner, 1993; Kresse and Furthmüller, 1996) (with valence configurations Fe-$3p^63d^74s^1$ and Mg-$2p^63s^2$), and a planewave cut-off of 400 eV. Exchange-correlation effects were treated in the generalized gradient approximation (GGA) with the Perdew–Wang scheme (Perdew and Wang, 1992). Single particle orbitals were populated according to Fermi–Dirac statistics. The Brillouin zone was initially sampled with the Γ-point; the energies were then corrected using energies sampled with a $3 \times 3 \times 2$ Monkhorst-Pack mesh. This correction can be expressed by

$$\Delta F^{G \rightarrow K} = \int_0^1 d\lambda \langle U^k - U^G \rangle_G \approx \langle U^k - U^G \rangle_G - \frac{1}{2k_B T}\langle \delta U^2 \rangle_G \tag{7}$$

where $\Delta F^{G \rightarrow K}$ is the correction from the Γ-point sampling to the multi-K-point sampling. U^G and U^K are the free energies of the Γ-point and
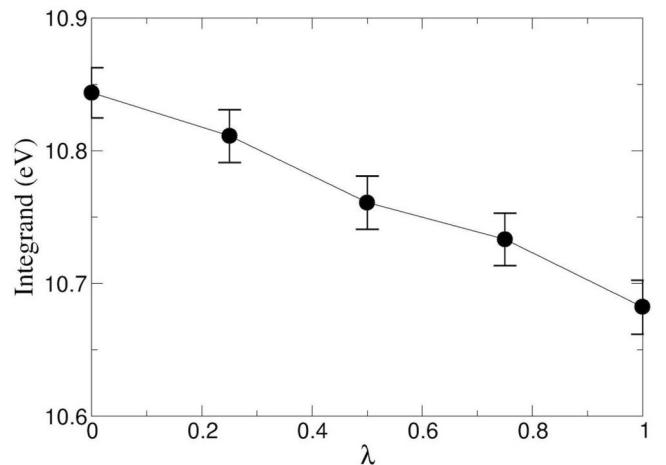

Fig. 1. The integrand $\langle U_1 - U_0 \rangle_\lambda$ in Eq. (4) as a function of λ used for calculating the free energy change $m(\overline{v},T,C_X)$ when $C_X = 0.03125$ in solid state. Filled circles indicate the AIMD data, and the bars indicate the statistical errors.

Table 1

Calculated chemical potentials (in eV) and partial atomic volumes (in Å^3) of Mg in Fe at 360 GPa and 6500 K, in comparison with those of S, Si and O (calculated at 370 GPa and 7000 K, (Alfè et al., 2002a)). The chemical potential of the solute in the low-concentration limit is expressed by $\mu_X(p,T,C_X) = k_B T ln C_X + \overline{\mu}_X(p,T,C_X)$, in which $(\overline{\mu}_X(p,T,C_X) = \mu_X^\dagger + \lambda_X(p,T)C_X)$. $\mu_{XA}^\dagger = \mu_X^\dagger - \mu_A^\dagger$, and $\mu_A^\dagger$ is the chemical potential of pure solvent Fe. Similarly, $\nu_{XA} = \nu_X - \nu_A$ with ν_A is the partial atomic volume of pure Fe. The superscripts l and s indicate the liquid and solid states, respectively.

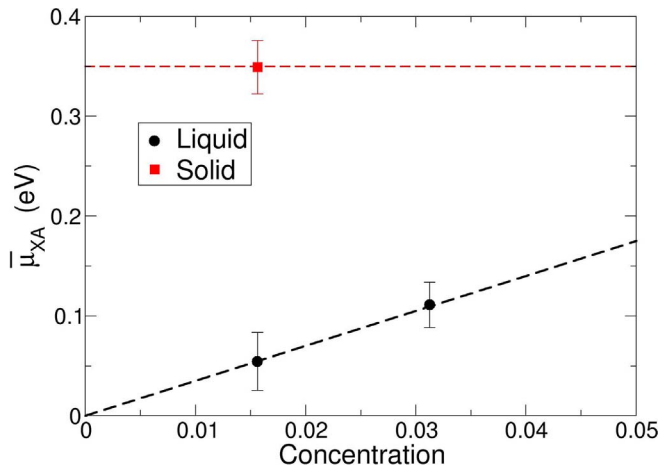| Solute	Mg	S	Si	O
$\mu_{XA}^{\dagger l}$	10.48 ± 0.03	3.5 ± 0.052	2.35 ± 0.05	-6.25 ± 0.2
λ_{XA}^{l}	0.91	6.15	3.6	3.25
ν_{XA}^{l}	0.06	-0.32	-0.32	-2.72
$\mu_{XA}^{\dagger s}$	10.80 ± 0.03	3.75 ± 0.05	2.40 ± 0.02	-3.65 ± 0.2
λ_{XA}^{s}		5.9	2.7	
ν_{X}^{s}	-0.13	-0.32	-0.32	-2.35

Fig. 2. The calculated chemical potential $\overline{\mu}_X(p,T,C_x)$ of Mg in solid and liquid Fe as a function of solute concentration C_x. The interaction between solutes makes $\overline{\mu}_X(p,T,C_x)$ dependent on C_x. The dashed line assumes a linear dependence $(\overline{\mu}_X(p,T,C_X) = \mu_X^\dagger + \lambda_X(p,T)C_X)$ in liquid by fitting the calculated data linearly, and such a dependence is currently not detectable in solid.

multi-K-point calculations, respectively. δU is

$$\delta U = \langle U^k - U^G - \langle U^k - U^G \rangle_G \rangle_G \qquad (8)$$

100 snapshots spaced by 50 steps were taken from the trajectories of the Γ-point calculations and the Brillouin zone was resampled with a $3 \times 3 \times 2$ Monkhorst-Pack mesh. The correction to the chemical potential is less 0.06 eV/impurity atom for the liquid and less than 0.3 eV/

impurity atom for the solid.

3. Results and discussion

We assume a linear mixing for the density of Fe-Mg alloys in the Fe-rich corner:

$$\rho = [(1 - C_{Mg})m_{Fe} + C_{Mg}m_{Mg}] / [(1 - C_{Mg})\nu_{Fe} + C_{Mg}\nu_{Mg}] \qquad (9)$$

At constant volume, the pressure change when replacing one Fe with Mg is $(\nu_{Mg} - \nu_{Fe})B_T/V$. Accordingly, we calculated the volume per atom of Mg in liquid and solid Fe. Mg has a partial atomic volume of 7.06 Å^3 in liquid Fe and 6.77 Å^3 in the solid. The partial atomic volume of Mg is smaller than Fe (6.9 Å^3) in solid Fe and bigger than Fe (7.0 Å^3) in liquid Fe. However, the differences are quite small in both cases. The partial atomic volume of Mg is similar to Si and S in Fe, and, therefore, is unlikely to create significant strain in the *hcp* lattice (Alfè et al., 2002a).

The calculated chemical potentials of Mg in solid and liquid Fe are shown in Table 1, with those of S, Si and O shown for comparison. We also plot the chemical potentials of Mg in Fig. 2. The difference between the chemical potentials of Mg in solid and liquid Fe is about 0.3 eV, which is smaller than $k_B T$ and also very close to that of S or Si (Alfè et al., 2002a). This implies that the partitioning of Mg between solid and liquid Fe will be similar to that of S and Si.

The calculated concentrations of Mg in solid Fe and the corresponding partition coefficients under core conditions are shown in Table 2. As can be seen in Table 2, the partition coefficient C_s/C_l is 0.57 when there is 0.5 mol.% Mg in liquid Fe. This increases slowly with the increasing concentration of Mg in the liquid, allowing a significant amount of Mg to partition into the solid inner core. If we assume 1.5 mol.% Mg in the outer core (suggested by the present day estimates of Badro et al. (2016)), we can expect about 0.9 mol.% Mg in the inner core. Recent studies (Dubrovinskaia et al., 2005; O'Rourke and Stevenson, 2016; Takafuji et al., 2005; Wahl and Militzer, 2015) suggest that there may be even more Mg in the outer core, possibly as much as 7.8 mol.%. Therefore, Mg may have visible effects on inner-core properties such as the density and seismic velocities. Indeed, as shown in Table 2, the addition of Mg into solid Fe decreases the density: 0.9 mol.% Mg in solid Fe can bring down the density by about 0.5%, which, for a density deficit away from pure iron of 4%, is a 13% contribution.

We can also consider whether Mg can contribute to the inner core boundary (ICB) density jump. The density jump across the ICB that is correlated with the ICB topography and compositional variance is not well constrained (Bolt and Qamar, 1970; Dziewonski and Anderson, 1981; Koper and Pyle, 2004; Masters and Shearer, 1990; Shearer and Masters, 1990; Tkalčić et al., 2009). Tkalčić et al. (2009) suggests a variance of density jump from 0.2 to 1.1 g/cm^3 depending on regional

Table 2

Calculated partition coefficients of Mg and the corresponding molar fractions in the solid at 360 GPa and 6500 K, with respect to specific concentrations of Mg in liquid Fe. The error is within 10%.

	Molar fraction (mol.%)										
C_l	0	0.005	0.010	0.015	0.020	0.025	0.030	0.035	0.040	0.045	0.050
C_s	0	0.003	0.006	0.009	0.012	0.015	0.018	0.021	0.025	0.028	0.031
	Partition coefficient										
C_s/C_l	/	0.57	0.58	0.58	0.59	0.59	0.60	0.61	0.61	0.62	0.63
	Density (g/cm^3)										
Liquid	13.248	13.210	13.172	13.134	13.100	13.058	13.020	12.982	12.944	12.906	12.868
Solid	13.440	13.418	13.397	13.375	13.354	13.329	13.307	13.285	13.256	13.234	13.212

differences. Other observations are as low as 0.45 g/cm^3 (Koper and Pyle, 2004) and as high as 1.8 g/cm^3 (Bolt and Qamar, 1970). As shown in Table 2, the partitioning of Mg between liquid and solid Fe provides a density jump that is not dissimilar from the density jump obtained between liquid and solid pure Fe when there is not much Mg in the core. However, the contribution of Mg to the inner-core outer-core (IC-OC) density jump will increase with increasing concentration of Mg in the core. Given the estimate of 1.1 wt% MgO (corresponding to 1.5 mol. % Mg) in the present outer core (Badro et al., 2016), Mg contributes 0.049 g/cm^3 to the density jump, which accounts for 3% in the lower bound (Bolt and Qamar, 1970) and 25% in the upper bound (Tkalčić et al., 2009). As such, Mg does not contribute significantly to the inner-core outer-core density jump compared to other light-element candidates like S and Si, unless more Mg exists in the core.

4. Conclusions

Using the combined techniques of AIMD and thermodynamic integration, we have calculated the chemical potential of Mg in solid and liquid Fe, and the corresponding partition coefficients under the extreme conditions relevant to the Earth's core. We find that Mg behaves in a similar way to Si and S, and a significant fraction of Mg can partition into solid Fe. Since recent studies suggest the solubility of Mg in Fe increases dramatically with increasing temperature and pressure, the concentration of Mg in the core could reach up to several percent (7.8 mol.%). Therefore, we can expect that Mg has a visible and significant effect on the inner-core properties such as the density and seismic velocities. However, the partitioning of Mg between liquid and solid Fe at these low concentrations of Mg means it is unlikely to contribute significantly to the IC-OC density jump, unless far larger amounts of Mg exist in the core. Further work is now required to establish if there is an Fe-Mg-X alloy that simultaneously matches the density and seismic velocities of the inner core.

Acknowledgments

Appendix A. Supplementary data

Supplementary data associated with this article can be found, in the online version, at http://dx.doi.org/10.1016/j.pepi.2017.12.003.

References

Alfè, D., Gillan, M.J., Price, G.D., 2000Ea. Constraints on the composition of the Earth's core from *ab initio* calculations. Nature 405 (6783), 172–175.

Alfè, D., Price, G.D., Gillan, M.J., 2000Eb. Thermodynamic stability of Fe/O solid solution at inner-core conditions. Geophys. Res. Lett. 27 (16), 2417–2420.

Alfè, D., Gillan, M.J., Price, G.D., 2002Ea. *Ab initio* chemical potentials of solid and liquid solutions and the chemistry of the Earth's core. J. Chem. Phys. 116 (16), 7127–7136.

Alfè, D., Gillan, M.J., Price, G.D., 2002Eb. Composition and temperature of the Earth's core constrained by combining *ab initio* calculations and seismic data. Earth Planet. Sci. Lett. 195 (1), 91–98.

Badro, J., Brodholt, J.P., Piet, H., Siebert, J., Ryerson, F.J., 2015. Core formation and core composition from coupled geochemical and geophysical constraints. Proc. Natl. Acad. Sci. 112 (40), 12310–12314.

Badro, J., Siebert, J., Nimmo, F., 2016. An early geodynamo driven by exsolution of mantle components from Earth's core. Nature 536 (7616), 326–328.

Blöchl, P.E., 1994. Projector augmented-wave method. Phys. Rev. B 50 (24), 17953.

Bolt, B.A., Qamar, A., 1970. Upper bound to the density jump at the boundary of the Earth's inner core. Nature 228 (5267), 148–150.

Di Tolla, F.D., Ronchetti, M., 1993. Applicability of Nosé isothermal reversible dynamics. Phys. Rev. B 48 (3), 1726.

Dubrovinskaia, N., et al., 2005. Beating the miscibility barrier between iron group elements and magnesium by high-pressure alloying. Phys. Rev. Lett. 95 (24), 245502.

Dziewonski, A.M., Anderson, D.L., 1981. Preliminary reference Earth model. Phys. Earth Planet. Inter. 25 (4), 297–356.

Koper, K.D., Pyle, M.L., 2004. Observations of PKiKP/PcP amplitude ratios and implications for Earth structure at the boundaries of the liquid core. J. Geophys. Res.: Solid Earth 109, B03301.

Kresse, G., Furthmüller, J., 1996. Efficiency of *ab-initio* total energy calculations for metals and semiconductors using a plane-wave basis set. Comput. Mater. Sci. 6 (1), 15–50.

Kresse, G., Hafner, J., 1993. *Ab initio* molecular dynamics for open-shell transition metals. Phys. Rev. B 48 (17), 13115.

Kresse, G., Joubert, D., 1999. From ultrasoft pseudopotentials to the projector augmented-wave method. Phys. Rev. B 59 (3), 1758.

Li, Y., Vočadlo, L., Brodholt, J., Wood, I., 2016. Thermoelasticity of Fe$_7$C$_3$ under inner core conditions. J. Geophys. Res.: Solid Earth 121 (8), 5828–5837.

Litasov, K., Shatskiy, A., 2016. Composition of the Earth's core: a review. Russ. Geol. Geophys. 57 (1), 22–46.

Martorell, B., Wood, I.G., Brodholt, J., Vočadlo, L., 2016. The elastic properties of hcp-Fe$_{1-x}$Si$_x$ at Earth's inner-core conditions. Earth Planet Sci. Lett. 451, 89–96.

Masters, T., Shearer, P., 1990. Summary of seismological constraints on the structure of the Earth's core. J. Geophys. Res.: Solid Earth 95 (B13), 21691–21695.

McDonough, W.F., Sun, S.S., 1995. The composition of the Earth. Chem. Geol. 120 (3), 223–253.

Nosé, S., 1984. A unified formulation of the constant temperature molecular dynamics methods. J. Chem. Phys. 81 (1), 511–519.

O'Rourke, J.G., Stevenson, D.J., 2016. Powering Earth's dynamo with magnesium precipitation from the core. Nature 529 (7586), 387–389.

Perdew, J.P., Wang, Y., 1992. Accurate and simple analytic representation of the electron-gas correlation energy. Phys. Rev. B 45 (23), 13244–13249.

Poirier, J.-P., 1994. Light elements in the Earth's outer core: a critical review. Phys. Earth Planet. Inter. 85 (3), 319–337.

Shearer, P., Masters, G., 1990. The density and shear velocity contrast at the inner core boundary. Geophys. J. Int. 102 (2), 491–498.

Takafuji, N., Hirose, K., Mitome, M., Bando, Y., 2005. Solubilities of O and Si in liquid iron in equilibrium with (Mg, Fe) SiO3 perovskite and the light elements in the core. Geophys. Res. Lett. 32 (6).

Tkalčić, H., Kennett, B.L.N., Cormier, V.F., 2009. On the inner–outer core density contrast from PKiKP/PcP amplitude ratios and uncertainties caused by seismic noise. Geophys. J. Int. 179 (1), 425–443.

Wahl, S.M., Militzer, B., 2015. High-temperature miscibility of iron and rock in terrestrial planet formation. Earth Planet Sci. Lett. 410, 25–33.